Research article

Mohsin Habib, Daria Briukhanova, Nekhel Das, Bilge Can Yildiz and Humeyra Caglayan*

Controlling the plasmon resonance via epsilon-near-zero multilayer metamaterials

https://doi.org/10.1515/nanoph-2020-0245
Received April 21, 2020; accepted July 11, 2020; published online July 26, 2020

Abstract: Localized plasmon resonance of a metal nanoantenna is determined by its size, shape and environment. Here, we diminish the size dependence by using multilayer metamaterials as epsilon-near-zero (ENZ) substrates. By means of the vanishing index of the substrate, we show that the spectral position of the plasmonic resonance becomes less sensitive to the characteristics of the plasmonic nanostructure and is controlled mostly by the substrate, and hence, it is pinned at a fixed narrow spectral range near the ENZ wavelength. Moreover, this plasmon wavelength can be adjusted by tuning the ENZ region of the substrate, for the same size nanodisk (ND) array. We also show that the difference in the phase of the scattered field by different size NDs at a certain distance is reduced when the substrate is changed to ENZ metamaterial. This provides effective control of the phase contribution of each nanostructure. Our results could be utilized to manipulate the resonance for advanced metasurfaces and plasmonic applications, especially when precise control of the plasmon resonance is required in flat optics designs. In addition, the pinning wavelength can be tuned optically, electrically and thermally by introducing active layers inside the hyperbolic metamaterial.

Keywords: epsilon near zero; hyperbolic metamaterial; localized surface plasmon; pinning effect.

1 Introduction

In the last two decades, a new frontier has been opened up with plasmonics. An enormous range of technological development has become possible by perfect light absorption, controlled propagation to certain directions or light confinement within a subwavelength volume [1–4]. Plasmonic light confinement has been utilized in biosensors [5–8], cellular imaging devices [9], surface-enhanced Raman spectroscopy [10] and nanoplasmonic rulers [11, 12]. To enable these applications, light is trapped around subwavelength metal nanoantennas at the localized surface plasmon resonance (LSPR) wavelength [13, 14], with enhanced electric fields. Size, shape, composition and arrangement of nanoantennas, as well as the dielectric environment surrounding them, have been extensively studied to obtain precise control over the LSPR [15, 16]. However, substrates were overlooked in these studies since mostly dielectric substrates, e.g. glass or silicon, were used. Metallic substrates were employed only in limited applications, such as hybridization between localized and propagating surface plasmons [17] or refractive index sensing [18].

One of the unusual materials of a growing interest is an epsilon-near-zero (ENZ) material, characterized by its permittivity (ε) being close to zero at certain wavelengths. These materials have been utilized in beam shaping and steering [19, 20], subwavelength tunnelling [21, 22] and enhanced nonlinear interactions [23]. Only recently, ENZ materials were used as substrates to control the LSPR of plasmonic antennas [24–27], revealing their great potential for plasmon-ENZ systems. However, only transparent conductive oxides, such as indium tin oxide and aluminium-doped zinc oxide, are used in these studies. These are naturally occurring ENZ materials with ENZ wavelengths in near-infrared and mid-infrared (MIR) regions [28]; hence, applications involving these materials are limited to those wavelength ranges. On the other hand, noble metals, such as gold (Au) and silver (Ag), have real permittivities Re(ε) close to zero in the ultraviolet region with very high imaginary permittivities (Im(ε)), preventing them from being effective ENZ materials. However, it is possible to engineer an effective material capable of supporting a vanishingly small permittivity in the desired wavelength range. A metamaterial composed of alternating layers of metal and dielectric was previously

***Corresponding author: Humeyra Caglayan**, Faculty of Engineering and Natural Sciences, Photonics, Tampere University, 33720 Tampere, Finland, E-mail: humeyra.caglayan@tuni.fi. https://orcid.org/0000-0002-0656-614X
Mohsin Habib, Daria Briukhanova, Nekhel Das and Bilge Can Yildiz: Faculty of Engineering and Natural Sciences, Photonics, Tampere University, 33720 Tampere, Finland. https://orcid.org/0000-0002-6109-9468 (M. Habib)

demonstrated to exhibit ENZ in the visible region [29–31] with a potential of ultrafast tuning [32]. Metamaterials with this geometry are known as hyperbolic metamaterials (HMMs) due to their hyperbolic wave-vector diagram [30].

In this work, by employing HMMs as ENZ substrates, we experimentally demonstrate how to control LSPR of a plasmonic nanoantenna array without changing its dimensions in the visible region. We present that not only the plasmon resonance wavelength can be pinned, although the nanodisk (ND) diameter is changed, but also it can easily be adjusted to another operating wavelength by changing the material composition of the substrate without any changes in the ND array. Furthermore, we show the effect of an ENZ substrate on the phase of the scattered field from different size NDs. This modification over the plasmon resonance relaxes the requirements on precise control of subwavelength features and provides flexibility in the design of the plasmonic nanostructures in flat optics applications by giving another option for tuning or compensating the fabrication errors.

The HMM substrates used in this study are composed of three bilayers of Au and titanium dioxide (TiO_2). The optical properties of these metamaterials are modelled by the effective medium theory (EMT) [30, 33–38]. The HMM serves as a uniaxial medium with permittivity given by a tensor $\varepsilon = [\varepsilon_{xx}, \varepsilon_{yy}, \varepsilon_{zz}]$, where in-plane isotropic/parallel components are defined as $\varepsilon_{xx} = \varepsilon_{yy} = \varepsilon_{\parallel}$. The third component which is out of the plane (perpendicular component) is defined as $\varepsilon_{zz} = \varepsilon_{\perp}$. The parallel and perpendicular components of permittivity of a medium composed of alternating thin layers of metal and dielectric are defined as follows:

$$\varepsilon_{\parallel} = \rho\varepsilon_m + (1-\rho)\varepsilon_d \tag{1}$$

$$\varepsilon_{\perp} = \frac{\varepsilon_m\varepsilon_d}{\rho\varepsilon_d + (1-\rho)\varepsilon_m} \tag{2}$$

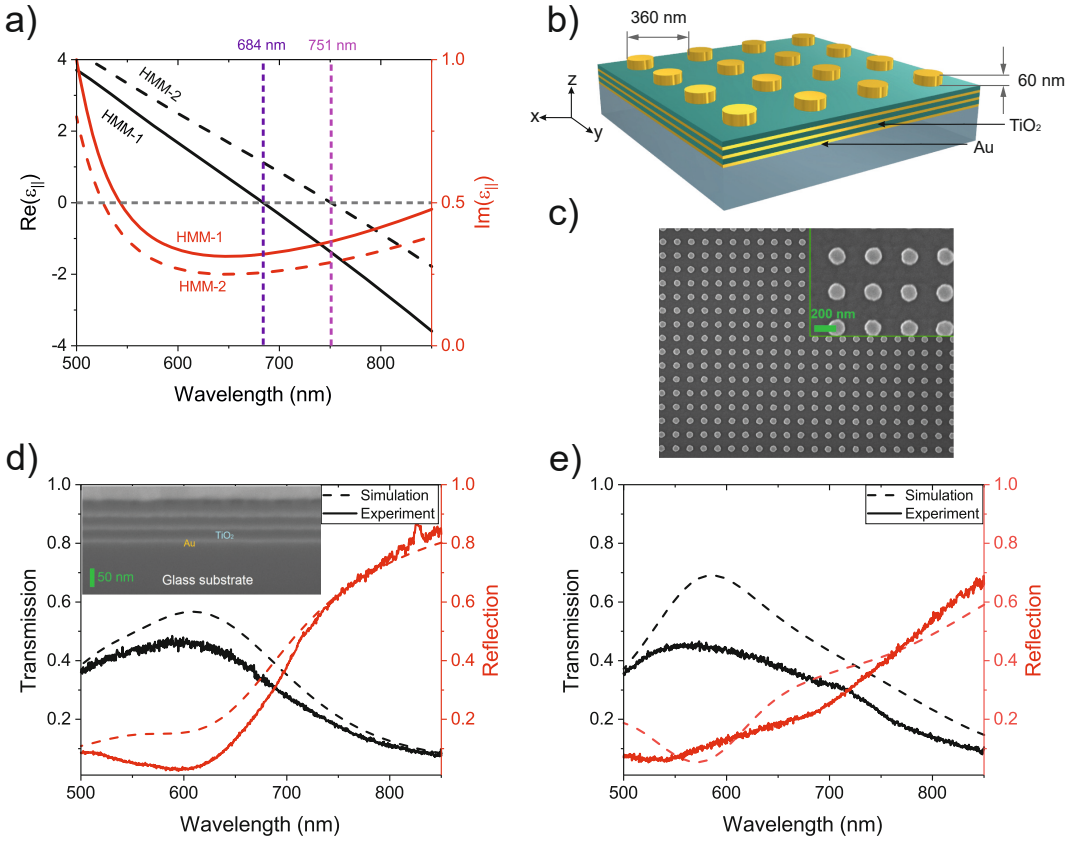

Figure 1: (a) The Re($\varepsilon_{\parallel}$) (black lines) and Im($\varepsilon_{\parallel}$) (red lines) of HMM-1 (solid lines) and HMM-2 (dashed lines). The crossover of Re($\varepsilon_{\parallel}$) for HMM-1 (violet dotted line) and HMM-2 (magenta dotted line) are highlighted. (b) The schematic of NDs on HMM and (c) the scanning electron microscopy (SEM) image of NDs on HMM-1. The simulated (dashed lines) and measured (solid lines) spectra of transmission (black lines) and reflection (red lines) results for (d) HMM-1 and (e) HMM-2. The inset of (d) shows the SEM image of HMM-1. HMM, hyperbolic metamaterial; ND, nanodisk.

where $\rho = t_m/(t_m + t_d)$ is the metal filling fraction, with $t_{m(d)}$ being the thickness of the metal (dielectric) layer, and ε_m and ε_d are permittivity values of metal and dielectric, respectively [30]. At specific wavelengths, a component of the permittivity tensor of the metamaterial either passes through zero (ENZ) or a resonant pole (epsilon-near-pole). The multilayer HMM shows the ENZ properties when the real part of $\varepsilon_\parallel$ ($\mathrm{Re}(\varepsilon_\parallel)$) component crosses zero and imaginary component ($\mathrm{Im}(\varepsilon_\parallel)$) is very small [30]. It is important to note that both dielectric and metallic nature of the substrate can affect the plasmon resonance significantly [18]. However, the substrate with ENZ properties results in slowing down of the resonance shift which is defined as pinning effect [26, 27].

In order to explore this, we designed two substrates which are referred as HMM-1 and HMM-2 and studied their effect on the plasmon resonance at their corresponding ENZ regions. Au thickness is 10 nm for both of them, but TiO_2 thickness is 25 nm for HMM-1, whereas 45 nm for HMM-2, providing the ENZ conditions at 684 and 751 nm, respectively. Figure 1(a) shows numerically calculated $\mathrm{Re}(\varepsilon_\parallel)$ and $\mathrm{Im}(\varepsilon_\parallel)$ using Equation 1. The $\mathrm{Re}(\varepsilon_\perp)$ and $\mathrm{Im}(\varepsilon_\perp)$ are calculated using Eq (2) and presented in SI-Figure 5. The simulated and measured transmission and reflection spectra of HMM-1 and HMM-2 (Figure 1(d) and 1(e)) are in good agreement with the projection of the calculated permittivity values. Finite-difference time-domain (FDTD) simulations were performed in Lumerical FDTD Solutions (see Methods for details).

2 Results and discussion

In this study, a set of ND arrays of increasing diameters on different substrates is investigated. Schematic of one of the ND arrays is presented in Figure 1(b). The diameter of the NDs is changed from 120 to 180 nm, while the thickness is kept 60 nm. Figure 2 shows the evolution of the calculated nanoantenna resonances (transmission dip) with increasing diameter on different substrates (glass, HMM-1 and HMM-2).

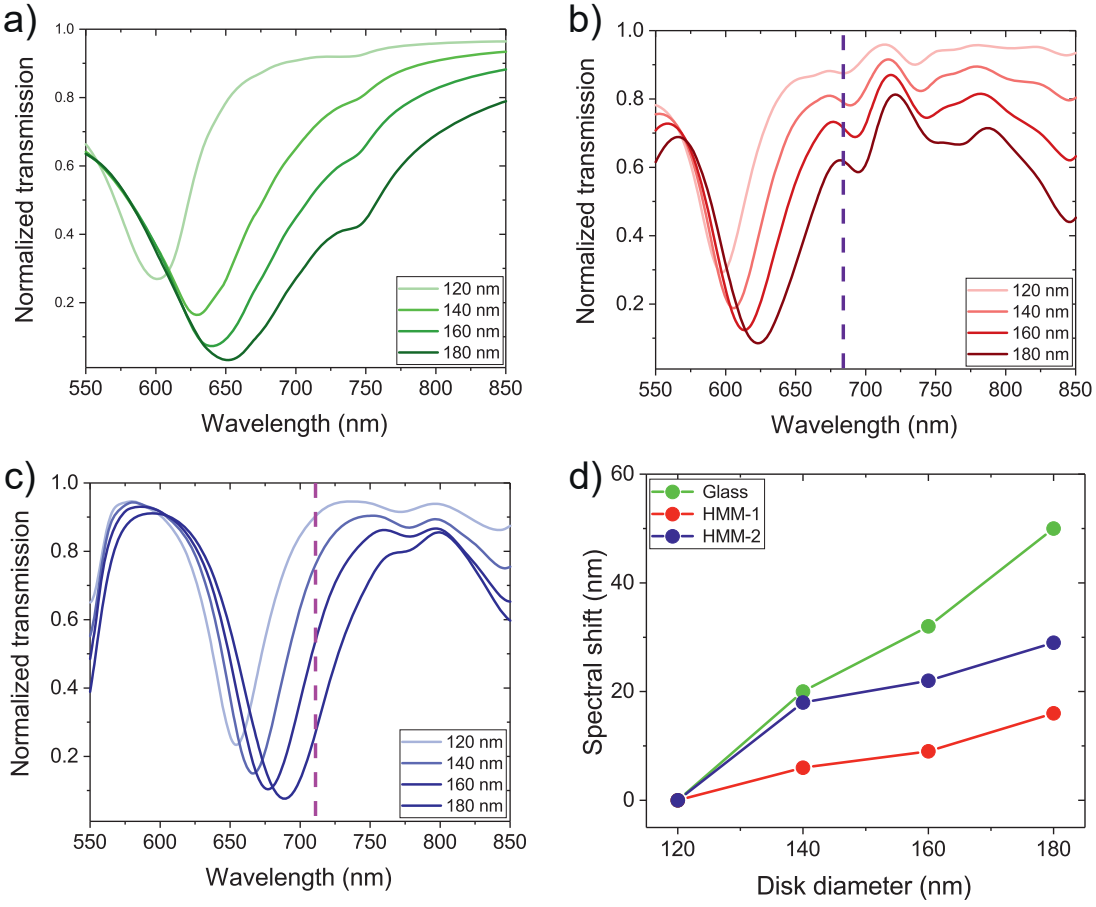

Figure 2: Evolution of the plasmon resonance with varying diameters of NDs on (a) glass (b) HMM-1, (c) HMM-2 and (d) spectral shift of the resonance, calculated by FDTD simulations. FDTD, finite-difference time-domain; HMM, hyperbolic metamaterial; ND, nanodisk.

The comparison of the spectral shifts of the plasmon resonances reveals that the change is much smaller when the NDs are on the ENZ substrates, compared to the case of the glass substrate. That is to say, the resonance of the NDs on the ENZ substrates is pinned near the ENZ wavelengths. Moreover, the ENZ substrates having different ENZ wavelengths control the pinning effect at those wavelengths.

To observe the pinning effect experimentally, we fabricated ND arrays on glass, HMM-1 and HMM-2 substrates using standard electron-beam lithography (EBL) and lift-off process (see Methods for details). Figure 1(c) shows the scanning electron microscope (SEM) image of a fabricated sample on HMM-1. Transmission spectra of NDs on glass with different diameters are presented in Figure 3(a). A resonance shift from 628 to 678 nm is observed, by changing the disk diameter from 120 to 180 nm. The same amount of modification in the diameter for the NDs on HMM-1 changes the plasmon resonance only within a smaller wavelength region of 659 nm ≤ λ ≤ 675 nm, as shown in Figure 3(b). We note that the transmission spectra are normalized to the transmission of the HMM-1 without the NDs. The LSPR of the antenna is not only determined by its size anymore when it is located on the ENZ substrate. This phenomenon is a consequence of the interaction between the resonating antennas, as well as the ENZ substrate. It is also possible to obtain this effect for an antenna array of the same size, at a different wavelength region, by adjusting the composition of the substrate. When the ND array is on HMM-2 having an ENZ wavelength at 751 nm, the pinning effect is observed in the region 703 nm ≤ λ ≤ 732 nm, as shown in Figure 3(c). The pinning effect is observed around the ENZ region of the corresponding HMM substrate.

Plasmonic nanoantennas scatter the incident field to all directions towards two different media: substrate and air. The relative efficiency of the scattering is determined by the dielectric constants of the two media. Therefore, effective permittivity of the local environment

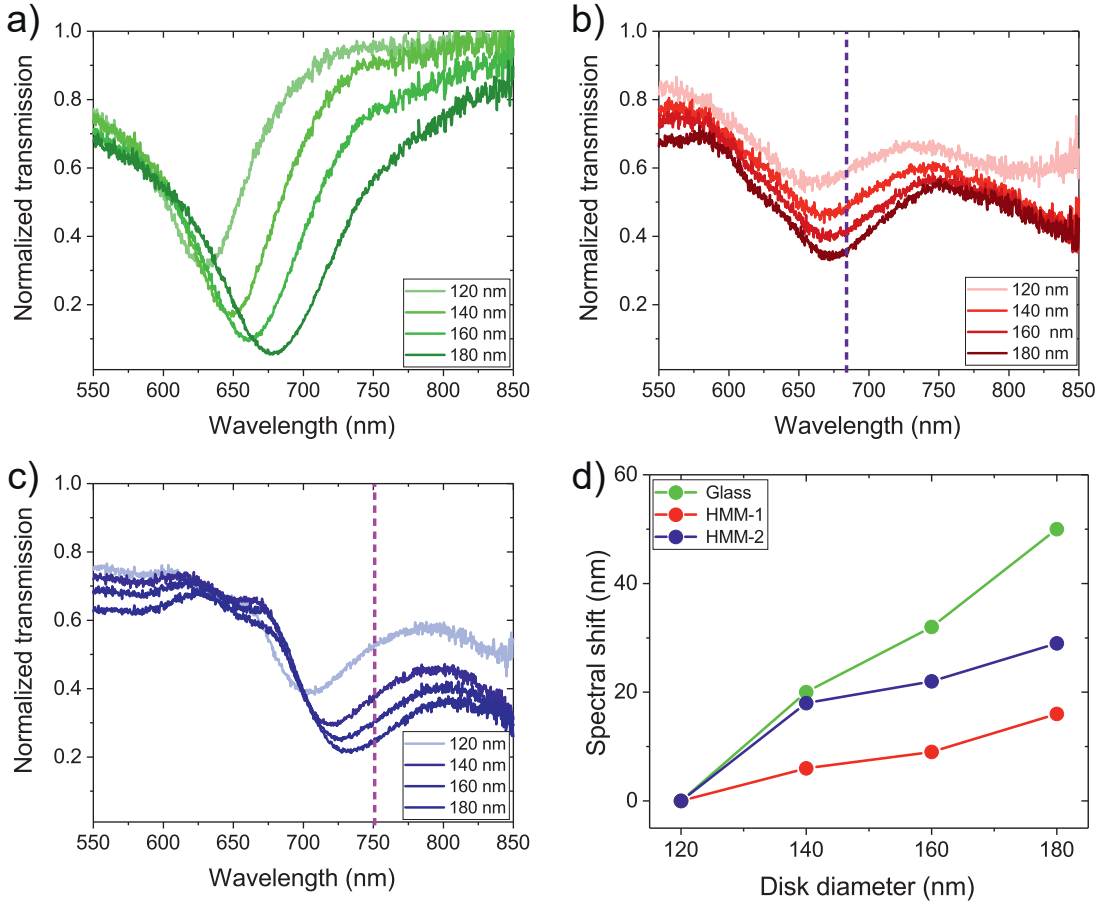

Figure 3: Normalized transmission spectra of the fabricated ND arrays, with disk diameters of 120, 140, 160 and 180 nm on three different substrates: (a) glass (green), (b) HMM-1 (red) and (c) HMM-2 (blue). The ENZ points of HMM-1 and HMM-2 are highlighted by violet and magenta vertical dashed lines in the associated graphs, respectively. (d) The spectral shifts in the resonance wavelengths of the NDs on glass, HMM-1 and HMM-2. HMM, hyperbolic metamaterial; ND, nanodisk; ENZ, epsilon-near-zero.

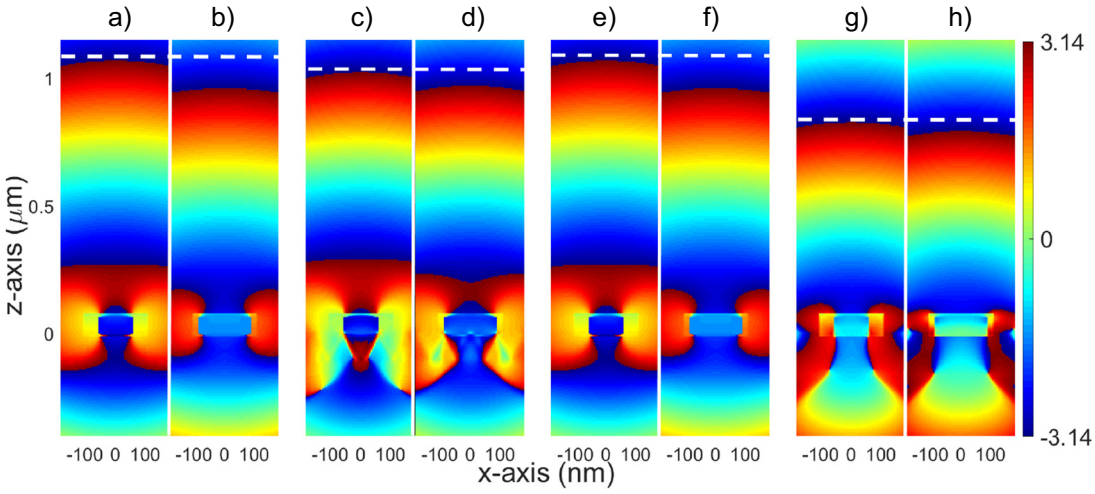

Figure 4: Phase profiles (in the unit of radian) of x component of the scattered E-field up to 2λ from the NDs of diameters (a) 120 nm and (b) 180 nm on glass at λ = 684 nm and (c) 120 nm and (d) 180 nm on HMM-1 at 684 nm. Similarly, (e) 120 nm and (f) 180 nm on glass at λ = 751 nm and (g) 120 nm and (h) 180 nm on HMM-2 at λ = 751 nm. White dotted lines are added for better visual comparison. HMM, hyperbolic metamaterial; ND, nanodisk.

can be defined as $\varepsilon_{\text{eff}} = (\varepsilon_{\text{sub}}+\varepsilon_{\text{air}})/2$. When the substrate is a low-loss ENZ medium, the value of the effective index $\left(n_{\text{eff}} = \sqrt{[\sqrt{\text{Re}(\varepsilon_{\text{eff}})^2 + \text{Im}(\varepsilon_{\text{eff}})^2} + \text{Re}(\varepsilon_{\text{eff}})]/2}\right)$ becomes almost zero at the ENZ region. The resonance frequency of an antenna can be approximated as $\lambda_{\text{res}} \simeq 2n_{\text{eff}}(D + 2\delta)$, where $D + 2\delta$ is the effective length of the antenna with a diameter (D) and evanescent extension of the resonant mode (δ) [26].

The vanishing index of refraction (reduced real permittivity) of the substrate limits the spectral shifting of the antenna resonance beyond the ENZ condition [26, 27]. Hence, when an antenna is on an ENZ substrate, an increase in the diameter of the ND antenna is compensated by small n_{eff}, reducing the amount of the shift in the LSPR near the ENZ wavelength, as observed in our experiments. The spectral shift in the plasmon resonance, with respect to the resonance wavelength of the ND arrays with 120 nm diameter, for each sample, is shown in Figure 3(d). The experimental results display a good agreement with the simulation results. The ND arrays on glass exhibit a total shift of 50 nm, whereas the shifts observed in the ND arrays on HMM-1 and HMM-2 are 16 and 29 nm, respectively. The shift in the resonance for HMM-1 is three times less than the one for glass. However, for HMM-2, it is half of the resonance shift obtained for the glass case. The shift in the resonance for HMM-1 is more suppressed compared to HMM-2 because the ENZ region of HMM-1 (660 nm ≤ λ ≤ 690 nm) is intentionally designed at the resonance wavelength of the antenna (on glass). On the other hand, the ENZ region (730 nm ≤ λ ≤ 780 nm) of HMM-2 is far away from the resonance of the antenna (on glass). The possibility to tune the ENZ region by simply changing the thickness of TiO_2 allows us to probe the pinning effect for HMM-1 and HMM-2 at two different wavelengths. Similar to the transmission minimum, the shift in the scattering peak of the ND antenna is suppressed three times for the ENZ substrates, compared to glass (see SI-Figure 8).

To further examine the scattering of NDs on different substrates, we calculate the phase of the x component of the scattered electric field (E-field) for the NDs of 120 and 180 nm diameter on glass and HMM-1 at 684 nm (Figure 4(a–d)) and on glass and HMM-2 at 751 nm (Figure 4(e–h)). The difference in the phase of the E-fields at a distance of ~2λ from the surface of the NDs (120 and 180 nm diameters) is 56 degrees when the substrate is glass. However, this difference reduces to 21 degrees when the substrate is changed to ENZ metamaterial. This provides possibilities for the effective control of the phase contribution of each nanostructure.

3 Conclusion and outlook

In conclusion, with this study, we reveal the effect of the ENZ metamaterials as a substrate. Due to the unique feature of ENZ media, we showed that one can diminish the effects of the size of the nanostructure on the spectral position of plasmon resonance. We present the pinning effect of HMM-based ENZ substrates on the LSPR of Au NDs. The plasmon resonance of the same ND is pinned at two different regions as a result of the substrates with different

ENZ wavelengths. Transmission spectra of the NDs, fabricated on glass, HMM-1 (ENZ at 684 nm) and HMM-2 (ENZ at 751 nm), display 50, 16 and 29 nm of spectral shifts in the resonance, respectively, as the disk diameter increases. The spectral shift of the NDs on HMMs is suppressed at least three times due to almost zero index of the substrate. Moreover, the phase of the scattered field from a ND is affected by the ENZ properties of the substrate providing flexibility on the phase modification.

Controlling the plasmonic resonance via substrate properties will open an entirely new avenue. For example, this will provide an efficient method to control the emission properties of quantum emitters and scattering properties of nanoparticles. We foresee that the improved low-loss ENZ substrates and dynamic tunability of the ENZ wavelength will bring more implementations to this platform. Recently, it has been shown that the large nonlinear optical response of ENZ materials [32, 39] provides optical tuning of ENZ wavelength. Similarly, the graphene-based tunable HMM [40] can be used in the MIR range to electrically tune the pinning wavelength. Another perspective would be using the function of vanadium dioxide as a phase-changing material in the HMM layers [41] to thermally turn on and off the pinning effect. The control over the plasmon resonance by designing an ENZ substrate and tuning its properties dynamically enables compensation of the fabrication error from visible to infrared region. Metal-insulator-metal–based tunable ENZ cavities [22] can be used to obtain a pinning effect in waveguides. Overall, these results may facilitate efficient sensing, better beam-steering applications and less cross-talk for on-chip nanophotonic devices in flat optics designs.

4 Methods

4.1 Numerical simulations

We use the commercially available software, Lumerical FDTD Solutions, for 3D electromagnetic simulations of transmission, reflection and field profiles of the samples. We use the experimental dielectric functions provided in the literature to model Au [42], SiO_2 [43] and TiO_2 [44]. HMM-1 and HMM-2 media are modelled with the help of dielectric functions obtained by effective medium approach, as shown in Figure 1(a). The overall thicknesses of the HMM-1 and HMM-2 media are 105 and 165 nm, respectively. The thickness of the NDs is 60 nm and the diameter is ranged from 120 to 180 nm. Conformal meshing is used in the simulations, while a finer mesh constraint to 4 nm is employed in the region enclosing the ND, to get a better resolution.

For the transmission and reflection simulations, the unit cell of size 360 nm is illuminated by a linearly (x) polarized plane wave source of wavelengths 500–900 nm. The boundary conditions (BCs) are set to periodic in the directions parallel to the source propagation (x, y) and perfectly matched layers (PMLs) in the direction perpendicular to the source propagation (z).

To simulate the scattered electric field profiles, the BCs are set to PMLs in all directions. We use a linearly (x) polarized plane wave source of wavelengths 500–900 nm. The source profile is obtained using the total-field scattered-field option (enclosing the ND). It separates the computation region into two distinct regions; one contains the total field (i.e. the sum of the incident and scattered fields), while the second region contains only the scattered field. A power monitor covering the whole simulation region is used to collect the scattered field at the ENZ wavelengths of each HMM.

4.2 Fabrication

For the fabrication of HMM substrates, the 500-μm-thick fused silica substrate is cleaned in acetone, isopropanol (IPA) with 10 min sonication and blow drying under nitrogen (N_2) flow. The plasma cleaning is used for thorough cleaning of organic contaminants from the surface. Once the samples are cleaned, 10 nm of Au and 25/45 nm of TiO_2 are deposited using electron beam deposition. About 1 nm of Ti is deposited before each gold layer to improve the adhesion at the rate of 0.5 Å/s. The SEM image of HMM-1 is obtained after focused ion beam milling, shown in the inset of Figure 1(d).

The periodic arrays of NDs are fabricated by standard EBL using 20 KeV and 10 μm aperture. The cleaned glass and fabricated HMM samples are spin coated with poly(methyl methacrylate) (PMMA)-A4 at 3000 rotation per minutes (rpm) for 40 s. The spin coated samples are baked at 180 C for 90 s in order to evaporate the anisole solution in PMMA-A4. The 100×100 μm^2 write field is used to create the NDs with the area dose of 300 μC/cm^2. The exposed samples are developed for 60 s in metylisobutylketon:IPA solution at the ratio of 1:3 and 30 s in IPA to stop the development process. The developed samples are loaded in the electron beam evaporation deposition chamber. Similar to HMM fabrication, 1 nm of Ti is used as an adhesion layer, followed by 60 nm of Au deposition at the rate of 0.5 Å/s. The S-1165 remover is used to lift off the metals, and the samples are left in the solution to heat up to 80 C. When the desired temperature is reached, the hot plate is turned off and the samples are kept in the solution for 5 min. Once the cracks start to appear in the metal thin films, the gentle stirring removes all the unwanted metal from the sample. The sample is rinsed in water, acetone and IPA and blow dried under N_2 flow to get rid of residual metal films. Four different matrices are fabricated for 120, 140, 160 and 180 nm disk size by changing the dose factor.

4.3 Optical characterization

Transmission spectra are measured using a Confocal Raman microscope from WiTec (alpha300R). The samples are excited with a broadband light source (Energetiq EQ-99XFC LDLS, spectrum 190–2100 nm). The optical beam is focused on the sample surface by using a 20× objective lens (ZEISS EC EPIPLAN 20X/0.4) at normal incidence. To detect the transmission spectra, a 50× objective lens (ZEISS EC EPIPLAN 50X/0.75) is placed at the back focal plane to collect transmitted light in the normal direction. The collected light is coupled to an optical fibre connected to a spectrometer (Ocean Optics Flame UV–VIS Spectrometer, detection range 40–900 nm). We first measure the transmission spectrum from the glass substrate. Then, we measure the transmission spectrum of the ND arrays, which is normalized to the

spectrum of glass. Similarly, the transmission spectra of the NDs on HMMs are normalized to transmission from HMM substrates.

Acknowledgement: The authors acknowledge the financial support of the European Research Council (Starting Grant project aQUARiUM; Agreement No. 802986) and Academy of Finland Flagship Programme (PREIN) (320165).
Author contribution: All the authors have accepted responsibility for the entire content of this submitted manuscript and approved submission.
Research funding: The authors acknowledge the financial support of the European Research Council (Starting Grant project aQUARiUM; Agreement No. 802986) and Academy of Finland Flagship Programme (PREIN) (320165).
Conflict of interest statement: The authors declare no conflicts of interest regarding this article.

References

[1] W. L. Barnes, A. Dereux, and T. W. Ebbesen, "Surface plasmon subwavelength optics," *Nature*, vol. 424, no. 6950, p. 824, 2003.
[2] E. Ozbay, "Plasmonics: merging photonics and electronics at nanoscale dimensions," *Science*, vol. 311, no. 5758, pp. 189–193, 2006.
[3] H. Raether, "Surface plasmons on smooth surfaces," in *Surface Plasmons on Smooth and Rough Surfaces and on Gratings*, Berlin, Heidelberg, Springer, 1988, pp. 4–39.
[4] P. Berini, R. Charbonneau, N. Lahoud, and G. Mattiussi, "Characterization of long-range surface-plasmon-polariton waveguides," *J. Appl. Phys.*, vol. 98, no. 4, p. 043109, 2005.
[5] A. G. Brolo, "Plasmonics for future biosensors," *Nat. Photonics*, vol. 6, no. 11, p. 709, 2012.
[6] H. Im, H. Shao, Y. I. Park, et al., "Label-free detection and molecular profiling of exosomes with a nano-plasmonic sensor," *Nat. Biotechnol.*, vol. 32, no. 5, p. 490, 2014.
[7] Y. Shen, J. Zhou, T. Liu, et al., "Plasmonic gold mushroom arrays with refractive index sensing figures of merit approaching the theoretical limit," *Nat. Commun.*, vol. 4, no. 1, pp. 1–9, 2013.
[8] J. Liu, M. Jalali, S. Mahshid, and S. Wachsmann-Hogiu, "Are plasmonic optical biosensors ready for use in point-of-need applications?," *Analyst*, vol. 145, no. 2, pp. 364–384, 2020.
[9] S. Lee, Y. Sun, Y. Cao, and S. H. Kang, "Plasmonic nanostructure-based bioimaging and detection techniques at the single-cell level," *TrAC-Trend Anal. Chem.*, vol. 117, pp. 58–68, 2019.
[10] J. E. Park, N. Yonet-Tanyeri, E. Vander Ende, et al., "Plasmonic microneedle arrays for in situ sensing with surface-enhanced Raman spectroscopy (SERS)," *Nano Lett.*, vol. 19, no. 10, pp. 6862–6868, 2019.
[11] B. M. Reinhard, M. Siu, H. Agarwal, A. Paul Alivisatos, and J. Liphardt, "Calibration of dynamic molecular rulers based on plasmon coupling between gold nanoparticles," *Nano Lett.*, vol. 5, no. 11, pp. 2246–2252, 2005.
[12] S. Lal, N. K. Grady, G. P. Goodrich, and N. J. Halas, "Profiling the near field of a plasmonic nanoparticle with Raman-based molecular rulers," *Nano Lett.*, vol. 6, no. 10, pp. 2338–2343, 2006.
[13] S. A. Maier and H. A. Atwater, "Plasmonics: localization and guiding of electromagnetic energy in metal/dielectric structures," *J. Appl. Phys.*, vol. 98, no. 1, p. 10, 2005.
[14] K. M. Mayer and J. H. Hafner, "Localized surface plasmon resonance sensors," *Chem. Rev.*, vol. 111, no. 6, pp. 3828–3857, 2011.
[15] M. Paul, "Not all that's gold does glitter," *MRS Bull.*, vol. 26, no. 12, pp. 1009–1014, 2001.
[16] E. Hao and G. C. Schatz, "Electromagnetic fields around silver nanoparticles and dimers," *J. Chem. Phys.*, vol. 120, no. 1, pp. 357–366, 2004.
[17] B. C. Yildiz, M. Habib, A. R. Rashed, and H. Caglayan, "Hybridized plasmon modes in a system of metal thin film–nanodisk array," *J. Appl. Phys.*, vol. 126, no. 11, p. 113104, 2019.
[18] B. Gerislioglu, L. Dong, A. Ahmadivand, H. Hu, P. Nordlander, and N. J. Halas, "Monolithic metal dimer-on-film structure: new plasmonic properties introduced by the underlying metal," *Nano Lett.*, vol. 20, no. 3, pp. 2087–2093, 2020.
[19] P. Moitra, Y. Yang, Z. Anderson, I. I. Kravchenko, D. P. Briggs, and J. Valentine, "Realization of an all-dielectric zero-index optical metamaterial," *Nat. Photonics*, vol. 7, no. 10, pp. 791–795, 2013.
[20] H. Hajian, E. Ozbay, and H. Caglayan, "Beaming and enhanced transmission through a subwavelength aperture via epsilon-near-zero media," *Sci. Rep.*, vol. 7, no. 1, pp. 1–8, 2017.
[21] M. G. Silveirinha and N. Engheta, "Theory of supercoupling, squeezing wave energy, and field confinement in narrow channels and tight bends using ε near-zero metamaterials," *Phys. Rev. B*, vol. 76, no. 24, p. 245109, 2007.
[22] V. Caligiuri, M. Palei, G. Biffi, S. Artyukhin, and R. Krahne, "A semi-classical view on epsilon-near-zero resonant tunneling modes in metal/insulator/metal nanocavities," *Nano Lett.*, vol. 19, no. 5, pp. 3151–3160, 2019.
[23] M. Z. Alam, S. A. Schulz, J. Upham, I. De Leon, and R. W. Boyd, "Large optical nonlinearity of nanoantennas coupled to an epsilon-near-zero material," *Nat. Photon.*, vol. 12, no. 2, p. 79, 2018.
[24] X. Duan, F. Zhang, Z. Qian, et al., "Accumulation and directionality of large spontaneous emission enabled by epsilon-near-zero film," *Optic Express*, vol. 27, no. 5, pp. 7426–7434, 2019.
[25] S. A. Schulz, A. A. Tahir, M. Z. Alam, J. Upham, I. De Leon, and R. W. Boyd, "Optical response of dipole antennas on an epsilon-nearzero substrate," *Phys. Rev.*, vol. 93, no. 6, p. 063846, 2016.
[26] J. Kim, A. Dutta, G. V. Naik, et al., "Role of epsilon-near-zero substrates in the optical response of plasmonic antennas," *Optica*, vol. 3, no. 3, pp. 339–346, 2016.
[27] C. T. DeVault, V. A. Zenin, A. Pors, et al., "Suppression of near-field coupling in plasmonic antennas on epsilon-near-zero substrates," *Optica*, vol. 5, no. 12, pp. 1557–1563, 2018.
[28] U. Koch, C. Hoessbacher, J. Niegemann, C. Hafner, and J. Leuthold, "Digital plasmonic absorption modulator exploiting epsilon-near-zero in transparent conducting oxides," *IEEE Photonics J.*, vol. 8, no. 1, pp. 1–13, 2016.
[29] J. Gao, L. Sun, H. Deng, C. J. Mathai, S. Gangopadhyay, and X. Yang, "Experimental realization of epsilon-near-zero metamaterial slabs with metal-dielectric multilayers," *Appl. Phys. Lett.*, vol. 103, no. 5, p. 051111, 2013.

[30] P. Shekhar, J. Atkinson, and Z. Jacob, "Hyperbolic metamaterials: fundamentals and applications," *Nano convergence*, vol. 1, no. 1, p. 14, 2014.
[31] R. Maas, J. Parsons, N. Engheta, and A. Polman, "Experimental realization of an epsilon-near-zero metamaterial at visible wavelengths," *Nat. Photon.*, vol. 7, no. 11, pp. 907–912, 2013.
[32] A. R. Rashed, B. C. Yildiz, S. R. Ayyagari, and H. Caglayan, "Hot electron dynamics in ultrafast multilayer epsilon-near-zero metamaterials," *Phys. Rev. B*, vol. 101, p. 165301, 2020.
[33] P. Alexander, I. Iorsh, P. A. Belov, and Y. Kivshar, "Hyperbolic metamaterials," *Nat. Photonics*, vol. 7, no. 12, p. 948, 2013.
[34] L. Ferrari, C. Wu, D. Lepage, X. Zhang, and Z. Liu, "Hyperbolic metamaterials and their applications," *Prog. Quant. Electron.*, vol. 40, pp. 1–40, 2015.
[35] C. L. Cortes, W. Newman, S. Molesky, and Z. Jacob, "Quantum nanophotonics using hyperbolic metamaterials," *J. Optic.*, vol. 14, no. 6, p. 063001, 2012.
[36] S. R. K. C. Indukuri, J. Bar-David, N. Mazurski, and U. Levy, "Ultrasmall mode volume hyperbolic nanocavities for enhanced light–matter interaction at the nanoscale," *ACS Nano*, vol. 13, no. 10, pp. 11770–11780, 2019.
[37] Z. Guo, H. Jiang, and H. Chen, "Hyperbolic metamaterials: from dispersion manipulation to applications," *J. Appl. Phys.*, vol. 127, no. 7, p. 071101, 2020.
[38] P. Huo, S. Zhang, Y. Liang, Y. Lu, and T. Xu, "Hyperbolic metamaterials and metasurfaces: fundamentals and applications," *Adv. Opt. Mater.*, vol. 7, no. 14, p. 1801616, 2019.
[39] M. Z. Alam, I. De Leon, and R. W. Boyd, "Large optical nonlinearity of indium tin oxide in its epsilon-near-zero region," *Science*, vol. 352, no. 6287, pp. 795–797, 2016.
[40] A. K. O. Mohamed, C. Guclu, and F. Capolino, "Graphene-based tunable hyperbolic metamaterials and enhanced near-field absorption," *Optic Express*, vol. 21, no. 6, pp. 7614–7632, 2013.
[41] S. Prayakarao, B. Mendoza, A. Devine, et al., "Tunable VO2/Au hyperbolic metamaterial," *Appl. Phys. Lett.*, vol. 109, no. 6, p. 061105, 2016.
[42] P. B. Johnson, and R.-W. Christy, "Optical constants of the noble metals," *Phys. Rev. B*, vol. 6, no. 12, p. 4370, 1972.
[43] I. H. Malitson, "Interspecimen comparison of the refractive index of fused silica," *Josa*, vol. 55, no. 10, pp. 1205–1209, 1965.
[44] J. R. DeVore, "Refractive indices of rutile and sphalerite," *JOSA*, vol. 41, no. 6, pp. 416–419, 1951.

Supplementary material: The online version of this article offers supplementary material (https://doi.org/10.1515/nanoph-2020-0245).